Supplemental Figure S1

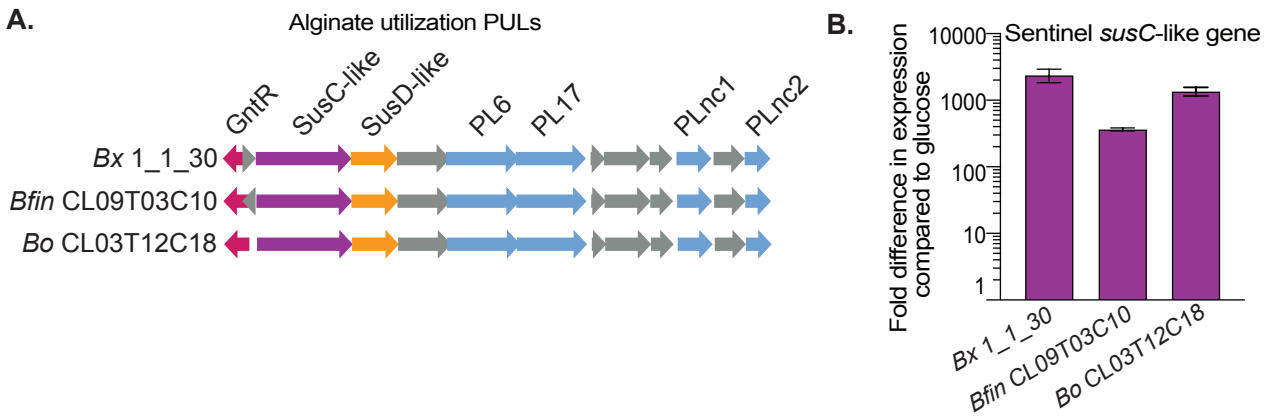

Figure S1. Organization and expression of Bacteroides alginate PULs. (**A.**) Polysaccharide utilization loci (PULs) involved in alginate utilization from strains of the 3 different species we found to utilize alginate in this study. These PULs contain two non-classified polysaccharide lyases (PL) labeled as PLnc1 and PLnc2. (**B.**) Expression of alginate responsive sentinel susC-like genes for representative strains by qPCR compared to glucose as a reference showing their strong responses to growth on alginate. Error bars are standard deviation (SD) of the mean. Three replicate cultures were performed. Corresponds to Figure 1.

Supplemental Figure S2

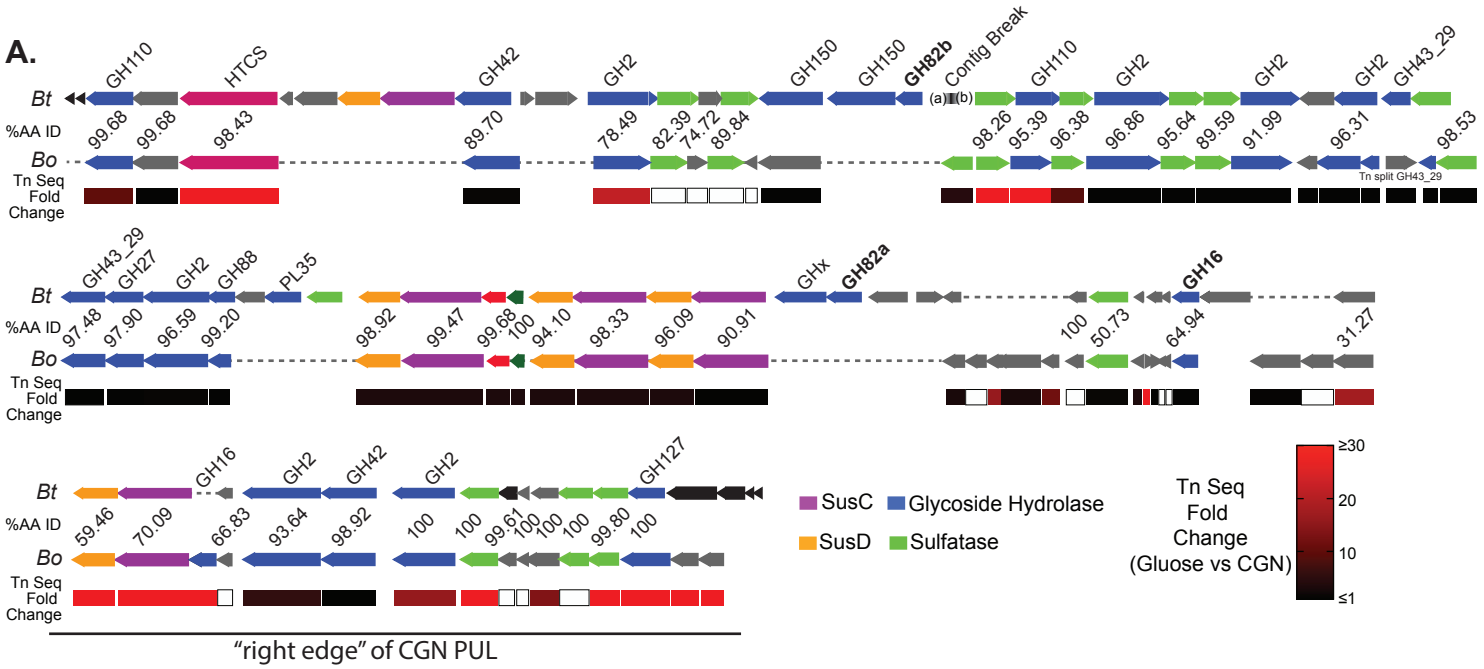

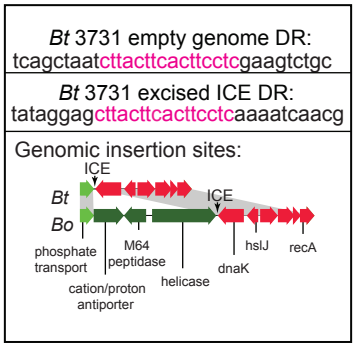

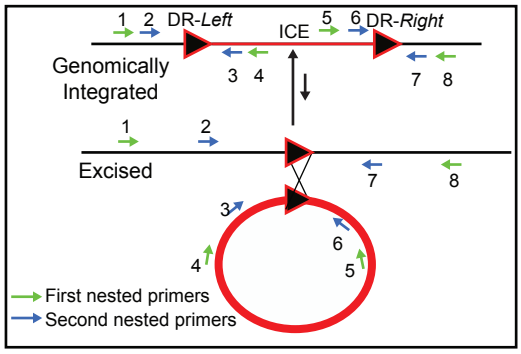

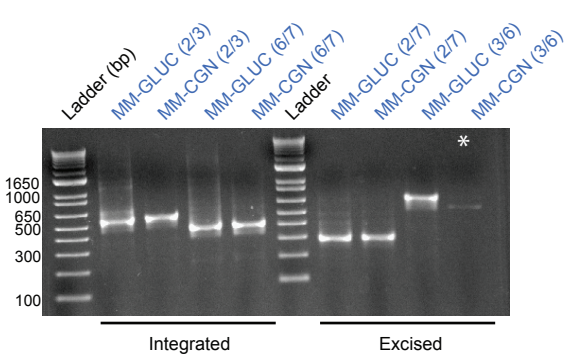

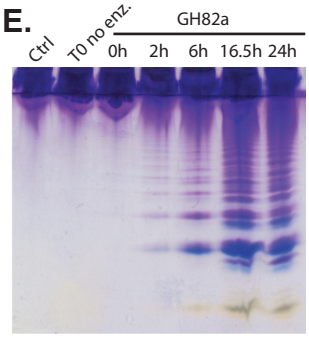

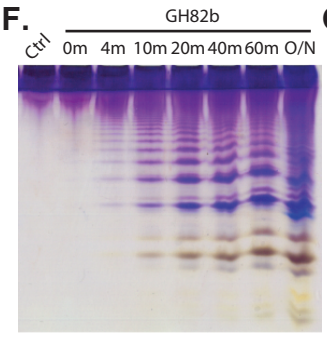

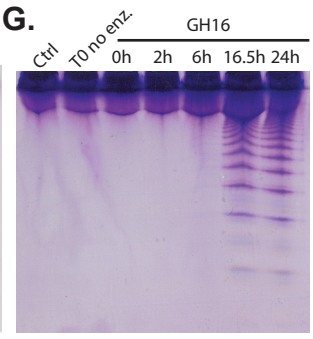

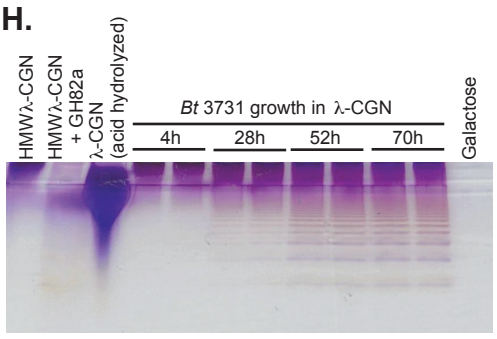

Figure S2. Gene organization, expression and activity of Bacteroides functions associated with carrageenan degradation. (**A.**) Schematics of the *Bt*^{3731} and *Bo*^{12C04} CGN-PULs highlighting the genes that are syntenic and/or homologous between the two loci. The dashed lines are included to align PUL genes and do not correspond to actual sequence. For shared genes, the percent amino acid identity is indicated by the numbers in between the PUL schematics. The TnSeq fold-change differences between glucose and carrageenan are represented by heat map at the bottom and only correspond to data gathered using the *Bo*^{12C04} isolate (Table S5). (**B.**) DNA sequencing results and corresponding genomic insertion site schematic for *Bt*^{3731} with pink nucleotides highlighting the direct repeat that mediates insertion. (**C.**) A schematic of the nested PCR approach used to examine possible ICE excision. (**D.**) Agarose gel showing the PCR products from the second round of the nested PCR for *Bt*^{3731} where both empty genome and excised products are produced indicative of ICE excision. Note that the prominent band in the last well (MM-CGN (3/6 primer set)) is a PCR artifact and not the excised ICE form (marked with *). (**E.**) C-PAGE analysis of products generated by the *Bt*^{3731} GH82a over time, showing a product profile consistent with endo activity. (**F.**) C-PAGE analysis of products generated by the *Bt*^{3731} GH82b over time, showing a product profile consistent with endo activity. (**G.**) C-PAGE analysis of products generated by the *Bt*^{3731} GH1a over time, showing a product profile consistent with endo activity (**H.**) C-PAGE analysis of production of lower molecular weight "poligeenan" oligo- and polysaccharides produced over time during Bt^{3731} growth (n=2) on 0.2% λ-CGN. The poligeenan pattern observed is similar to the product profile of GH82a digested λ-CGN as compared to untreated and acid hydrolysed λ-CGN. The last lane shows supernatant of *Bt*^{3731} grown for 52h in galactose medium to control for capsular polysaccharide or other products made by this strain. Gel was stained overnight using 0.005% Stains-All in 50% ethanol solution followed by destaining in 10% ethanol. Corresponds to Figure 2.

Supplementary Figure S3

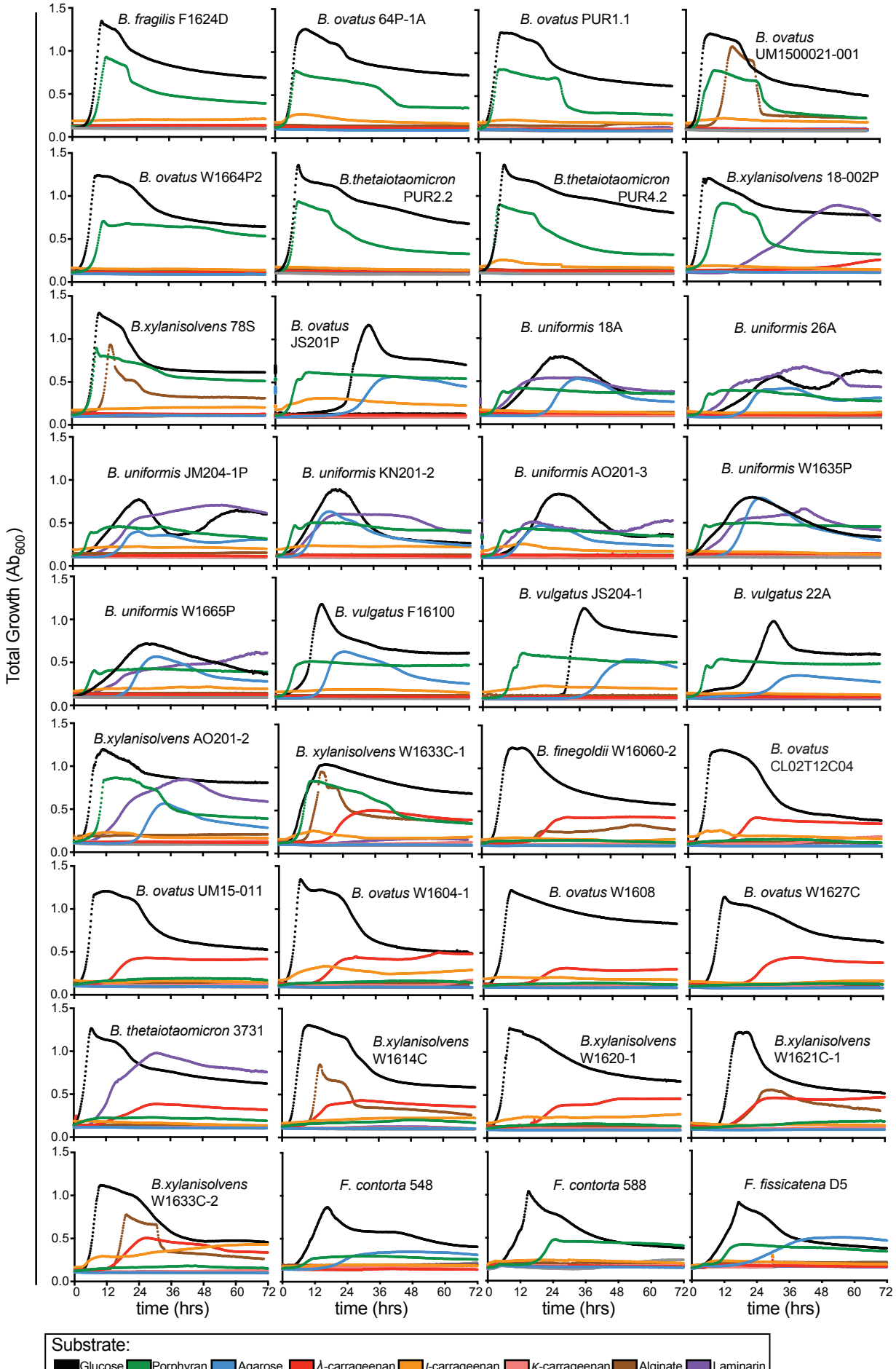

Figure S3. Growth of *Bacteroides* and *Faecalicatenum* isolates on seaweed polysaccharides. Growth curve analyses (mean of n=6 separate replicates) of seaweed degrading bacterial isolates on 7 different substrates, plus glucose as a control. Corresponds to Figures 1-5.

Supplementary Figure S4

A.

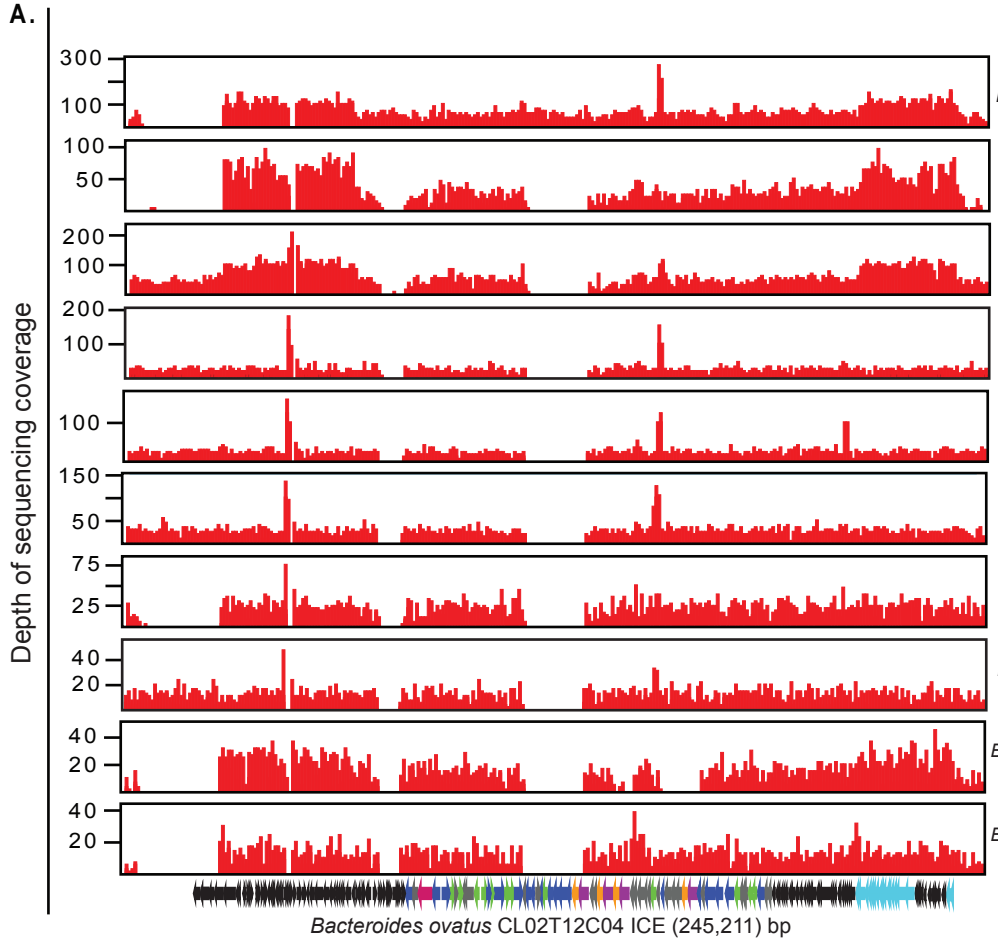

Strain	Coverage (%) ICE	Coverage (%) PUL	nt identity (%) ICE	nt identity (%) PUL
B. xylanisolvens W1633C-1	91	100	99.82	99.97
B. finegoldii W16060-2	79	82	98.90	99.49
B. ovatus UM15-011	88	82	99.61	99.44
B. ovatus W1604-1	88	82	99.74	99.44
B. ovatus W1608	88	82	99.74	99.47
B. ovatus W1627C	88	82	99.75	99.47
B. xylanisolvens W1614C	79	80	99.72	99.46
B. xylanisolvens W1620-1	85	79	99.77	99.51
B. xylanisolvens W1621C-1	70	62	99.00	99.00
B. xylanisolvens W1633C-2	77	79	99.76	99.56

B.

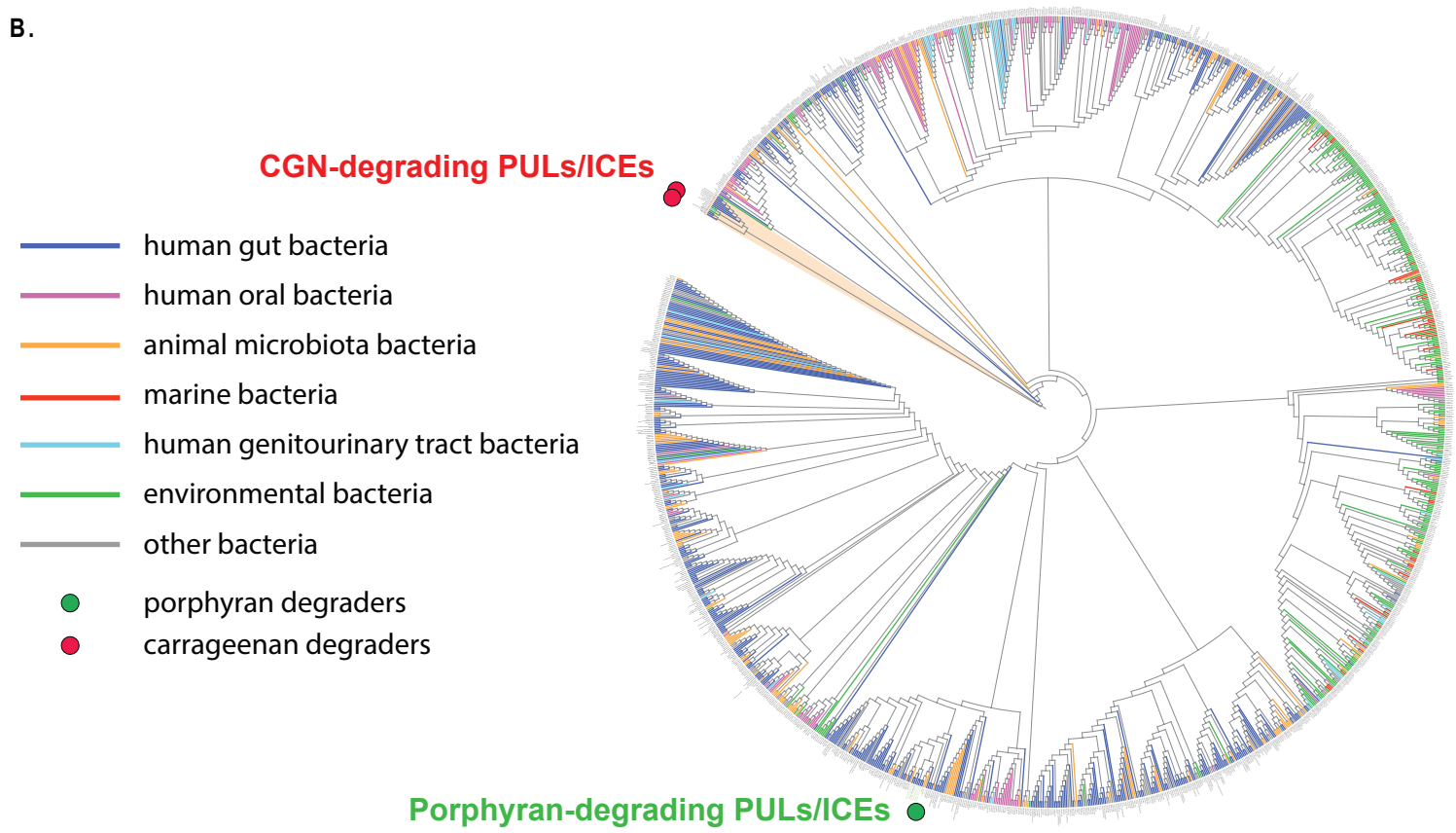

Figure S4. Identification of additional strains with PULs similar to those found in *B. thetaiotaomicron* and *B. ovatus* and the relationship of their associated ICEs with that involved in mobilization of porphyran utilization functions. (**A.**) Histograms showing reference guided alignment of CGN-degrading strain genomes to the entire *Bo*^{12C04} CGN-ICE sequence. The ICE and PUL linear coverage and nucleotide identity of covered regions of the ICE and PUL are shown as percent identity on the right. (**B.**) A tree of 2,255 unique Bacteroidetes TraJ protein sequences from publicly available data and the new genomes reported here. The locations of the TraJ sequences associated with the *B. plebeius*-type porphyran ICE and the newly identified CGN ICE are highlighted with green and red circles, respectively, showing their distance. Corresponds to Figure 2.

Supplementary Figure S5

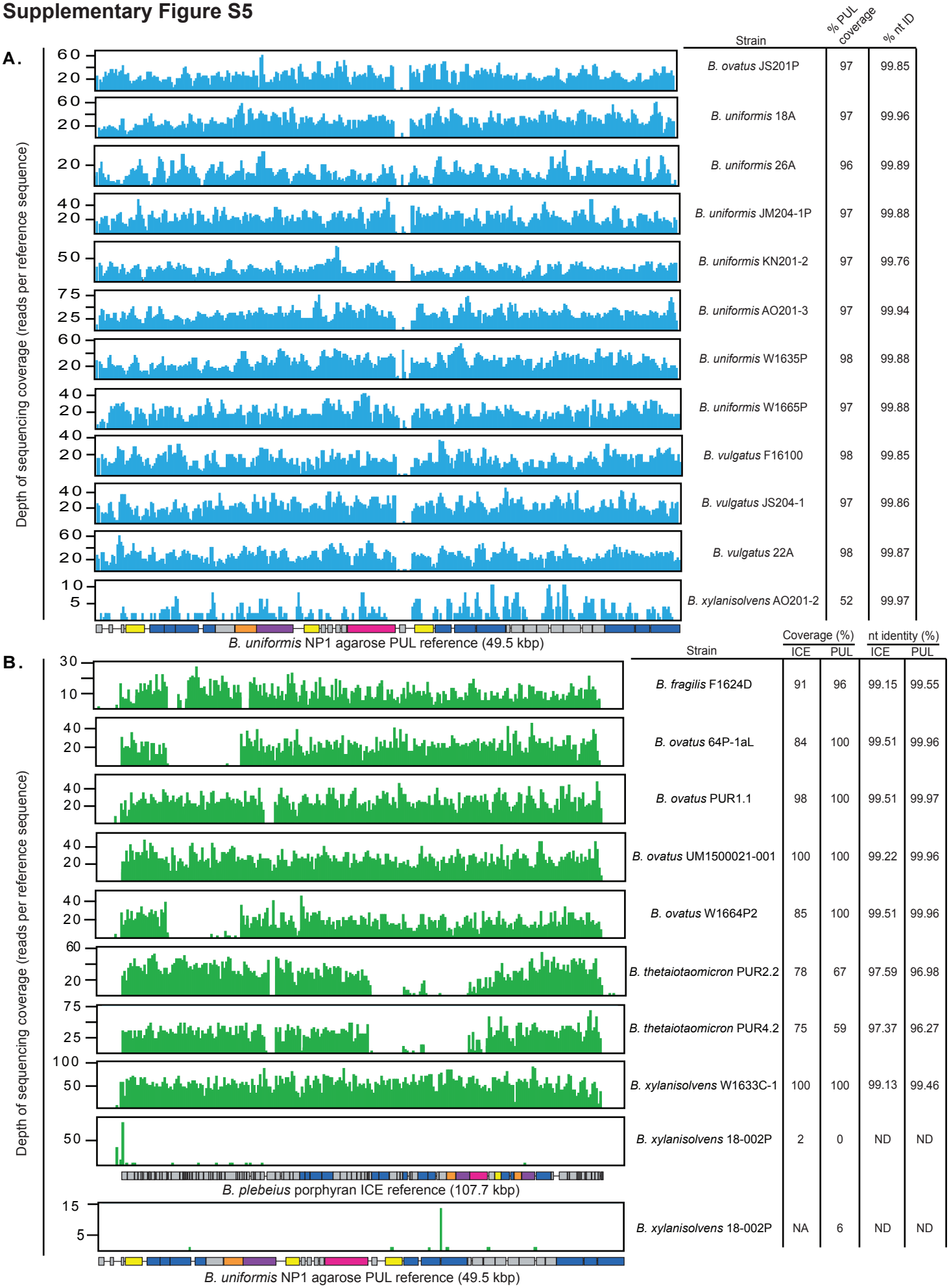

Strain	% PUL coverage	% nt ID
B. ovatus JS201P	97	99.85
B. uniformis 18A	97	99.96
B. uniformis 26A	96	99.89
B. uniformis JM204-1P	97	99.88
B. uniformis KN201-2	97	99.76
B. uniformis AO201-3	97	99.94
B. uniformis W1635P	98	99.88
B. uniformis W1665P	97	99.88
B. vulgatus F16100	98	99.85
B. vulgatus JS204-1	97	99.86
B. vulgatus 22A	98	99.87
B. xylanisolvens AO201-2	52	99.97

Strain	Coverage (%)		nt identity (%)	
	ICE	PUL	ICE	PUL
B. fragilis F1624D	91	96	99.15	99.55
B. ovatus 64P-1aL	84	100	99.51	99.96
B. ovatus PUR1.1	98	100	99.51	99.97
B. ovatus UM1500021-001	100	100	99.22	99.96
B. ovatus W1664P2	85	100	99.51	99.96
B. thetaiotaomicron PUR2.2	78	67	97.59	96.98
B. thetaiotaomicron PUR4.2	75	59	97.37	96.27
B. xylanisolvens W1633C-1	100	100	99.13	99.46
B. xylanisolvens 18-002P	2	0	ND	ND
B. xylanisolvens 18-002P	NA	6	ND	ND

Figure S5. Identification of additional strains with PULs similar to those found in *B. uniformis* and *B. plebeius* for agarose and porphyran utilization, respectively. (**A.**) Mapping of genomic reads from agarose-porphyran degrading strains to the *Bu*^{NP1} reference PUL showing linear coverage across the genomically inserted PUL and percent of coverage and nt identity. (**B.**) Mapping of genomic reads from porphyran degrading strains to the *Bp*^{17135} reference PUL showing linear coverage across the ICE and percent of coverage and nt identity. Mapping of the *Bx*$^{18\text{-}002P}$ assembly against the *Bu*^{NP1} reference is included at bottom to show the lack of homology to either of the known agarose or porphyran-degrading loci. Corresponds to Figures 3-4.

Supplementary Figure S6

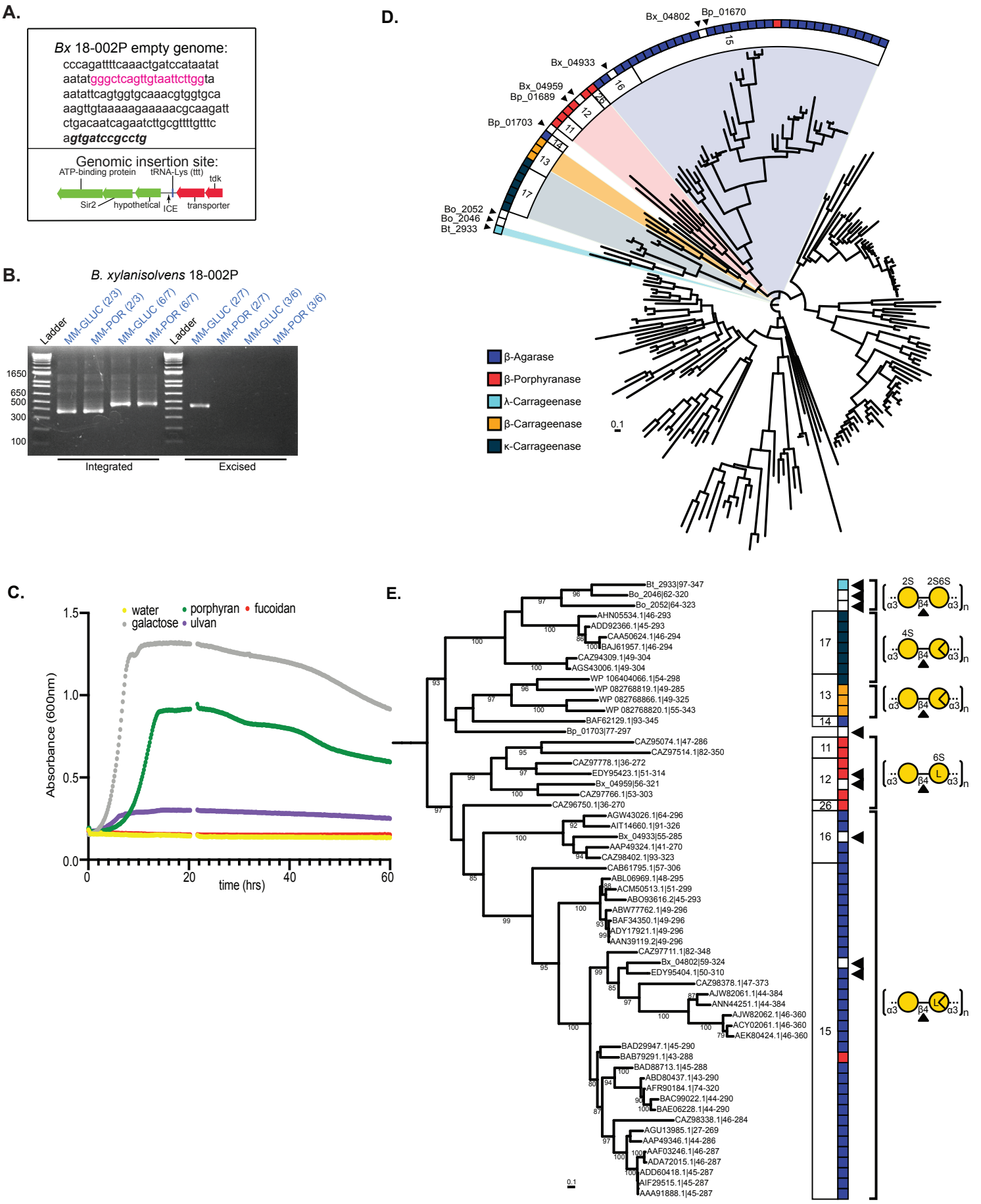

Figure S6. Characterization of a second mobilizable PUL associated with poprhyran degradation by human gut *Bacteroides*. (**A.**) DNA sequencing results and corresponding genomic insertion site schematic for $Bx^{18\text{-}002P}$ with pink nucleotides highlighting the direct repeat that presumably mediates insertion. (**B.**) Agarose gel showing the PCR products from the second round of the nested PCR for $Bx^{18\text{-}002P}$ where an empty genome product is formed indicating some amount of ICE excision. (**C.**) Growth analysis of Bx^{18002P} on two additional seaweed polysaccharides, ulvan and fucoidan, demonstrating lack of growth on these two polysaccharides. (**D.**) Phylogenetic comparison of GH16 enzymes from the Bt^{3731} and Bo^{12C04} CGN PULs, and the $Bx^{18\text{-}002P}$ and Bp^{17135} POR PULs against biochemically characterized GH16 members in the CAZy database. *Bt, Bo, Bx*, and *Bp* sequences are marked by black arrows. Characterized sequences of "red seaweed degrading" GH16 subfamilies (11-17, 26) are highlighted and members are colored by enzyme activity. (**E.**) The above tree is pruned to display accession numbers and illustrate products from glycosidic cleavage. Corresponds to Figure 4.

Supplementary Figure S7

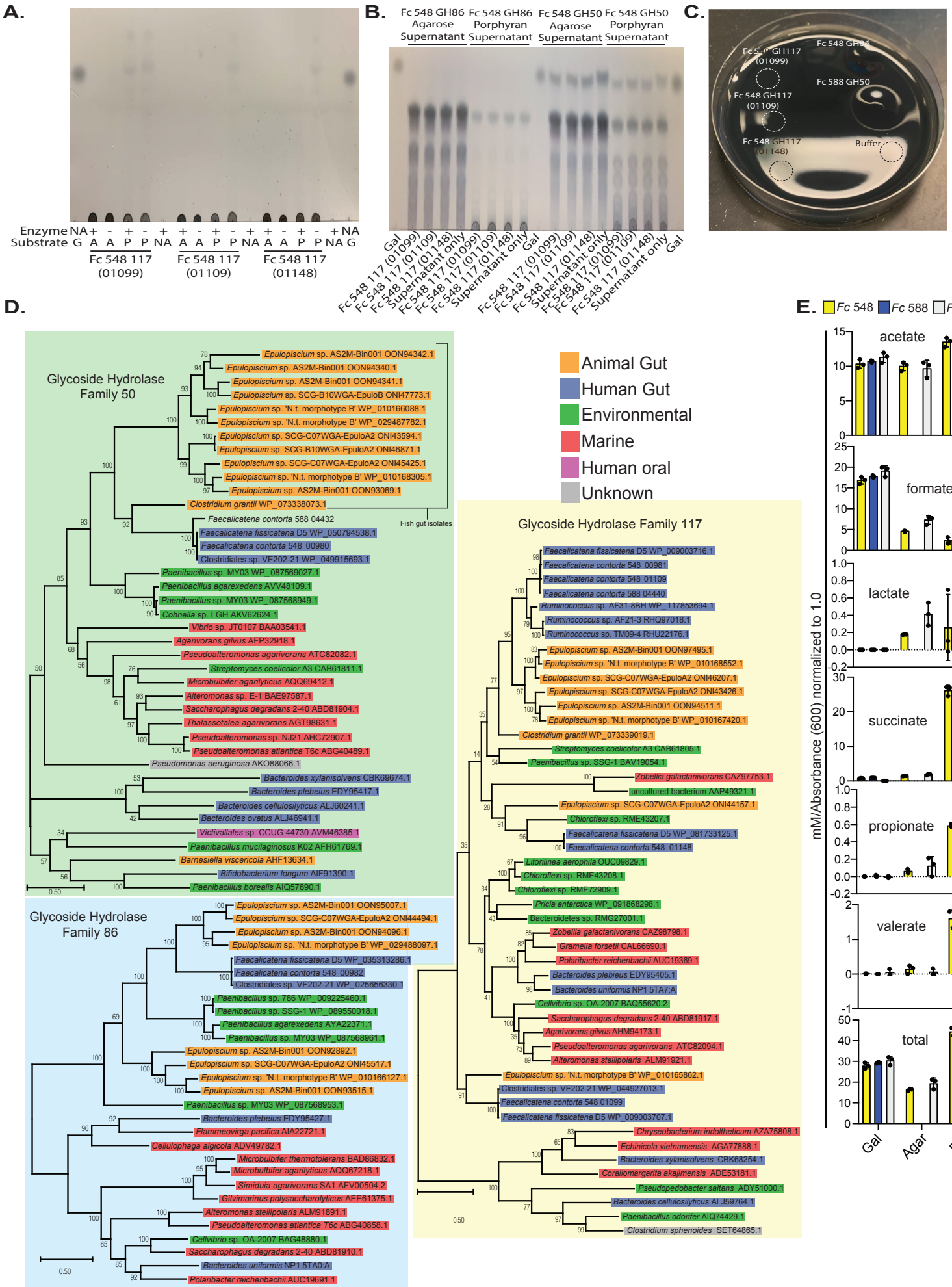

Figure S7. Activity and phylogeny of Faecalicatena enzymes that degrade agarose and porphyran. (**A.**) Thin-layer chromatography analysis of enzymatic reactions for 3 of 4 GH117 enzymes found in *Fc*^{548}. Minimal enzymatic activity is observed on agarose (A) and porphyran (P) substrates with galactose (G) as a reference. These enzymes are often neoagarooligosaccharide hydrolases targeting smaller agarose fragments. The fourth GH117 found in *Fc548* is 100% similar by amino acid sequence to one analyzed here and was therefore omitted from analysis. (**B.**) Thin-layered chromatography of enzyme reactions of the same GH117 enzymes in A., but incubated with the supernatants of the GH86 (**Fc**^{548}) and GH50 (*Fc*^{588}) reactions. No further degradation of the agarose or porphyran oligosaccharides is observed after GH117 treatment. (**C.**) An agar plate where the filter sterilized recombinant glycoside hydrolases from *Faecalicatena contorta* species were spot plated and incubated overnight at 37ºC. As observed with colonies growing on the same plates, the GH50 and GH86 display "pitting" even as pure enzymes, whereas the GH117 enzymes show little, if any, activity. (**D.**) Maximum-Likelihood phylogenic trees generated using deduced amino acid sequences of the GH50, GH86 and GH117 glycoside hydrolases from *Faecalicatena* spp. as well as similar sequences located by BLAST or present in the CAZY database and Protein Data Bank (PDB). Note that the *Faecalicatena* spp. enzymes are often in clades containing enzymes from the marine fish gut symbiont genera *Epulopiscium* and also *Paenibacillus* spp. environmental bacteria that have been isolated from marine sediments. Since the *Clostridiales* sp. VE202-21 enzymes clustered close to the *Faecalicatena* spp. enzymes, we searched public databases to find that this is also a *Faecelicatena contorta* strain. Three human gut *Ruminococcus* sp. enzymes also clustered closely to one of the GH117 enzymes from *Faecalicatena* spp. However, examination of these genomes provided little evidence for similar seaweed degrading phenotypes based on the surrounding genetic architecture. (**E.**) Metabolite analysis of *Faecalicatena* spp. grown on galactose, agarose and porphyran. The mM concentrations of each SCFA-BCFA were normalized to a media control and an OD_{600} of 1.0 for each strain and substrate. There is no *Fc*^{588} analysis on agarose as this strain does not grow on agarose. There was no detection of butyrate, isobutyrate or isovalerate in any sample. Error bars correspond to the standard error of the mean. Three replicate experiments were performed. Corresponds to Figure 5.